

Antarctic temperature and CO₂: near-synchrony yet variable phasing during the last deglaciation

Jai Chowdhry Beeman^{a,1}, Léa Gest^{a,1}, Frédéric Parrenin^a, Dominique Raynaud^a, Tyler J. Fudge^b, Christou Buizert^c, and Edward J. Brook^c

^aUniv. Grenoble Alpes, CNRS, IRD, IGE, F-38000 Grenoble, France

^bDepartment of Earth and Space Sciences, University of Washington, Seattle, WA 98195, USA

^cCollege of Earth, Ocean, and Atmospheric Sciences, Oregon State University, Corvallis, OR 97331, USA

¹Jai Chowdhry Beeman and Léa Gest contributed equally to this work.

Correspondence to: Frédéric Parrenin frederic.parrenin@univ-grenoble-alpes.fr

Abstract. The last deglaciation, which occurred from 18,000 to 11,000 years ago, is the most recent large natural climatic variation of global extent. With accurately dated paleoclimate records, we can investigate the timings of related variables in the climate system during this major transition. Here, we use an accurate relative chronology to compare regional temperature proxy data and global atmospheric CO₂ as recorded in Antarctic ice cores. We build a stack of temperature variations by averaging the records from five ice cores distributed across Antarctica, and develop a volcanic synchronization to compare it with the high-resolution, robustly dated WAIS Divide CO₂ record. We assess the CO₂ / Antarctic temperature phase relationship using a stochastic method to accurately identify the probable timings of abrupt changes in their trends. Four coherent changes are identified for the two series, and synchrony is within the 2 σ uncertainty range for all of the changes except the Holocene onset. During the large, millennial-scale changes at the onset of the last deglaciation at 18 ka and the onset of the Holocene at 11.5 ka, Antarctic temperature most likely led CO₂ by several centuries. CO₂ and Antarctic temperature peaked nearly synchronously at 14.4 ka, the onset of the Antarctic Cold Reversal (ACR) period. And CO₂ likely led Antarctic temperature by around 250 years at the end of the ACR. However, two significant changes, one at 16 ka in the CO₂ record and one after the ACR onset in the temperature record, do not have significant counterparts in the other record. The timings of changes in trends for the individual proxy records show variations from the stack, indicating some regional differences in the pattern of temperature change, particularly between West and East Antarctica. The likely-variable phasings we identify testify to the complex nature of the mechanisms driving the carbon cycle and Antarctic temperature during the deglaciation.

1 Introduction

Glacial-interglacial transitions, or deglaciations, mark the paleorecord approximately every 100,000 years over the past million years or so (Jouzel et al., 2007; Lisiecki and Raymo, 2005; Williams et al., 1997). The last deglaciation, often referred to as glacial termination 1 (T1), offers a case study for a large global climatic change, very likely in the 3-8°C range on the global scale (Masson-Delmotte et al., 2013), and thought to be initiated by an orbitally driven insolation forcing (Berger, 1978; Hays et al., 1976; Kawamura et al., 2007). The canonical interpretation of this apparent puzzle is that insolation acts

as a pacemaker of climatic cycles and the amplitude of glacial-interglacial transitions is mainly driven by two strong climatic feedbacks: atmospheric CO₂ and continental ice surface-albedo changes. However, the mechanisms that control the CO₂ rise are still a matter of debate. Accordingly, reconstructing the phase relationship (leads and lags) between climate variables and CO₂ during the last termination has become of importance, and has a substantial history in ice core research (Barnola et al., 1991; Caillon et al., 2003; Parrenin et al., 2013; Pedro et al., 2012; Raynaud and Siegenthaler, 1993).

Global temperature has been shown to lag CO₂ on average during T1 (Shakun et al., 2012), supporting the importance of CO₂ as an amplifier of orbitally-driven global-scale warming. But Antarctic temperature and CO₂ concentrations changed much more coherently as T1 progressed. Indeed, near the end of the glacial-interglacial transition, Antarctic warming slowed and even reversed during a period of about 2000 years, coinciding with a warm period in the North called the Bølling–Allerød (B/A). This period of cooling in Antarctica is called the Antarctic Cold Reversal (ACR). A period of cooling in the Northern Hemisphere known as the Younger Dryas (YD), followed the B/A, coinciding with a period of warming in the SH.

High-latitude Southern Hemisphere paleotemperature series—including Southern Ocean temperature—varied similarly to Antarctic temperature during T1 (Shakun et al., 2012; Pedro et al., 2016). Upwelling from the Southern Ocean is thought to have played an important role in the deglacial CO₂ increases. The Atlantic Meridional Overturning Current, or AMOC, a major conduit of heat between the Northern and Southern Hemispheres and component of the bipolar seesaw, the umbrella term encompassing the mechanisms thought to control the seemingly alternating variations of Northern and Southern Hemisphere temperature, is thought to have influenced Southern Ocean upwelling during the deglaciation (Marcott et al., 2014). A weakening of the oceanic biological carbon pump appears to have dominated the deglacial CO₂ increase until 15.5 ka, when rising ocean temperature likely began to play a role as well (Bauska et al., 2016).

Ice sheets are exceptional archives of past climates and atmospheric composition. Local temperature is recorded in the isotopic composition of snow/ice (Jouzel et al., 2007; NorthGRIP Project Members, 2004) due to the temperature dependent fractionation of water isotopes (Lorius and Merlivat, 1975; Johnsen et al., 1989). The concentration of continental dust in ice sheets is a proxy of continental aridity, atmospheric transport intensity and precipitation (Petit and Delmonte, 2009; Lambert et al., 2012). Finally, air bubbles enclosed in ice sheets are near-direct samples of the past atmosphere. However, the age of the air bubbles is younger than the age of the surrounding ice, since air is locked in at the base of the firn (on the order of 70 m below the surface on the West Antarctic Ice Sheet (WAIS) Divide) at the Lock-In Depth (LID) (Buizert and Severinghaus, 2016). The firn, from top to bottom, is composed of a convective zone (CZ) where the air is mixed vigorously, and a diffusive zone (DZ) where molecular diffusion dominates transport. Firn densification models can be used to estimate the LID and the corresponding age difference (Sowers et al., 1992).

Atmospheric CO₂ concentrations, recorded in the air bubbles enclosed in ice sheets, are better preserved in Antarctic ice than in Greenland ice, because the latter has much higher concentrations of organic material and carbonate dust (Raynaud et al., 1993). Measured essentially on the Vostok and EPICA Dome C ice cores, the long ice core record of CO₂ (Lüthi et al., 2008) covers the last 800 ka. This record is of global significance.

Early studies suggested that at the initiation of the termination around 18 ka B1950 (kiloyears before 1950 A.D.), just after the Last Glacial Maximum (LGM), Antarctic temperature started to warm 800 ± 600 yr before CO₂ began to increase (Monnin

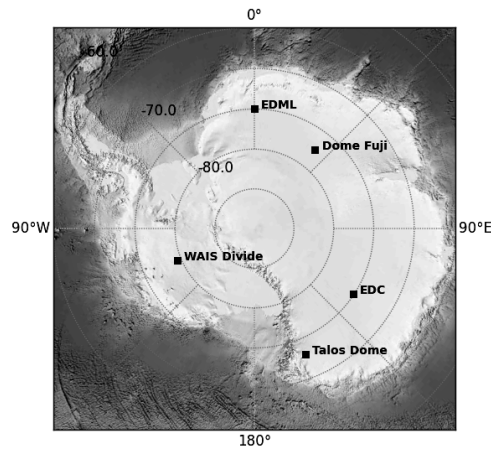


Figure 1. Drilling locations of the ice cores from which the CO₂ and isotopic paleotemperature records included in this study were measured.

et al., 2001), a result that was sometimes misinterpreted to mean that CO₂ was not an important amplification factor of the deglacial temperature increase. This study used measurements from the EPICA Dome C (EDC) ice core (Jouzel et al., 2007) and a firn densification model to determine the air chronology. However, this firn densification model was later shown to be
 30 in error by several centuries for low accumulation sites such as EDC during glacial periods (Loulergue et al., 2007; Parrenin et al., 2012).

Two more recent works (Pedro et al., 2012; Parrenin et al., 2013), used stacked temperature records and improved estimates of the age difference between ice and air records to more accurately estimate the relative timing of changes in Antarctic temperature and atmospheric CO₂ concentration. In the first of these studies, measurements from the higher accumulation
 35 ice cores at Siple Dome and Law Dome, used to decrease the uncertainty in the ice-air age shift, indicated that CO₂ lagged Antarctic temperature by 0-400 yr on average during the last deglaciation (Pedro et al., 2012). The second study (Parrenin et al., 2013) used measurements from the low accumulation EDC ice core but circumvented the use of firn densification models by using the nitrogen isotope ratio $\delta^{15}\text{N}$ of N₂ as a proxy of the DZ height, hypothesizing that the height of the CZ was negligible during the study period. CO₂ and Antarctic temperature were found to be roughly in phase at the beginning of TI and at the end
 40 of the ACR period, but CO₂ was found to lag Antarctic temperature by several centuries at the beginning of the Antarctic Cold Reversal and Holocene periods. However, the assumption that $\delta^{15}\text{N}$ reflects DZ height is imperfect, as it may underestimate the DZ height for sites with strong barometric pumping and layering (Buizert and Severinghaus, 2016).

A new CO₂ record of unprecedented high resolution (Marcott et al., 2014) from the WAIS Divide (WD) ice core merits the reopening of this investigation. The air chronology of WAIS Divide is well constrained thanks to a relatively high accumulation
 45 rate and to accurate nitrogen-15 measurements (Buizert et al., 2015). The WAIS record evidences centennial-scale changes in

the global carbon cycle during the last deglaciation superimposed on more gradual, millennial-scale trends that bear resemblance to Antarctic temperature (Marcott et al., 2014).

The deglacial temperature rise seen at WD is structurally similar to that at other Antarctic sites. However, West Antarctic warming may have been greater in magnitude than East Antarctic warming by up to 3 degrees, and the rise in West Antarctic temperature shows early warming starting around 21 ka B1950, following local insolation (Cuffey et al., 2016). This early warming trend is much more gradual in records from East Antarctic ice cores. The difference between the two records may be related to sea ice conditions around East and West Antarctica, and perhaps to elevation changes (Cuffey et al., 2016; WAIS Divide Project Members and others, 2013). However, the temperature record at WAIS Divide shows an acceleration in warming
5 around 18 ka B1950 which is also present in East Antarctic records (WAIS Divide Project Members and others, 2013).

On the much shorter timescales of the observable past, Jones et al. (2016) note differing temperature trends at the drilling sites of the five cores used in this study. On the other hand, the interpretation of individual isotopic records can prove complicated, as local effects, including those of ice sheet elevation change and sea ice extent, are difficult to correct.

In the present work we refine our knowledge of leads and lags between Antarctic temperature and CO₂. We develop a new
10 stack of accurately synchronized Antarctic temperature records to reduce local signals, placed using volcanic matching on the WAIS Divide chronology (WD2014). We then compare the temperature stack to the high resolution WAIS Divide CO₂ record by determining the probable timings of changes in trend, and calculate probable change point timings for the five individual isotope-derived records used in our stack as well.

2 Methods and data

15 2.1 Temperature stack and ice chronology

We develop a stack of isotopic temperature records (Antarctic Temperature Stack 2, or ATS2) in order to remove local influences and noise in the individual records to the greatest extent possible. Our stack contains five records: EDC, Dome Fuji (DF), Talos Dome (TALDICE), EPICA Dronning Maud Land (EDML) and WAIS Divide (WD). We use previously published volcanic ties between EDC, DF, TALDICE and EDML (Parrenin et al., 2013; Fujita et al., 2015). We then develop a volcanic
20 synchronization between the EDC and WD cores (Figure 2) to place our stack on the WD2014 chronology (Buizert et al., 2015; Sigl et al., 2016). The Vostok record, included in the stack used by Parrenin et al. (2013) is excluded: it contains additional chronological uncertainty as it is derived using records from two drilling sites.

The individual isotopic records are converted to temperature (deg C) corrected for source isotopic variations (Bintanja et al., 2013), resampled to a timestep of 20 years, and averaged. The standard deviation of the records at each timestep is assumed to
25 be representative of the uncertainty concerning the conversion from isotopes to temperature, and of the uncertainty rooted in the geographic distribution of the stack.

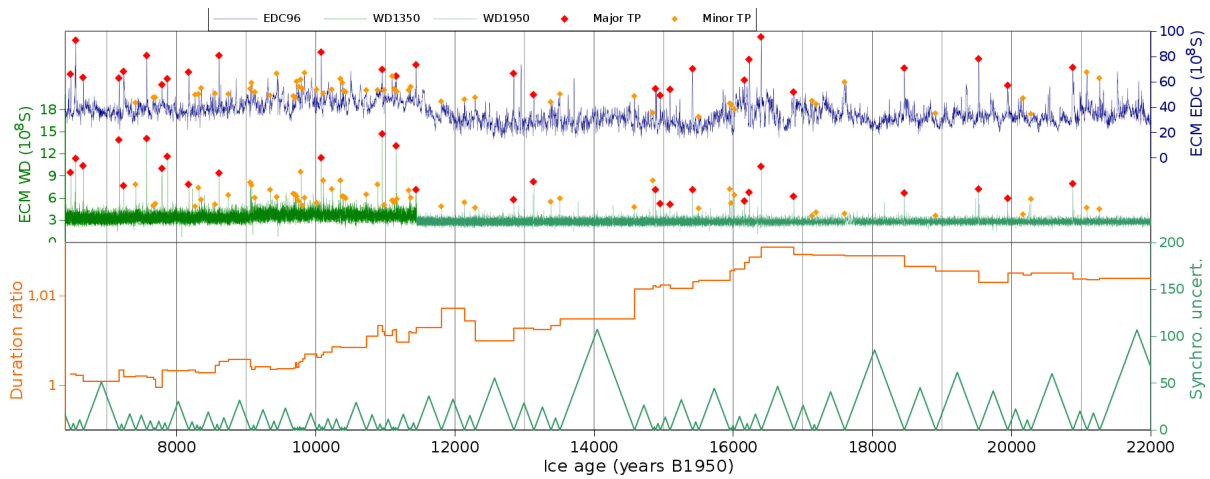


Figure 2. Volcanic synchronisation between the EDC and WD ice cores. (Top) ECM records from EDC (blue) and WD (raw data: 6.4–11.4 ka; adjusted data: 11.4–24 ka). Red diamonds show a primary set of synchronization points, selected in an initial round of visual synchronization. Orange diamonds are a secondary set of synchronization points, selected in a second round of visual synchronization. (Bottom) The ratio of the age difference between two consecutive pairs of tie points is shown in orange. The synchronization uncertainty, which is determined as 20% of the distance to the nearest tie point, is shown in green. This uncertainty is included in the calculation of leads and lags.

2.2 CO₂ and air chronology

We use atmospheric CO₂ data from the WD ice core Marcott et al. (2014) which consist of 1,030 measurements at 320 depths that correspond to ages between 23,000 and 9,000 years B1950 with a median resolution of 25 years. At WD, the age offset between the ice and air (trapped much later) at a given depth, Δage , is calculated using a firn densification model, which is constrained using nitrogen-15 data, a proxy for firn column thickness (Buizert et al., 2015). Δage ranges from 500 ± 100 yr at the last glacial maximum, to 200 ± 30 yr during the Holocene. Δage uncertainty is added to cumulative layer counting uncertainty to determine the total uncertainty of the air chronology.

2.3 Identifying changes in trend

We identify likely change points by taking the residuals of the linear interpolations between the change points with respect to the raw data (similarly to Parrenin et al. (2013)). At the base of our method is a parallelized Metropolis-Hastings (MH) procedure (Goodman and Weare, 2010; Foreman-Mackey et al., 2013). Therefore, we do not present a single “best fit” but rather analyze the ensemble of fits accepted by the routine. We plot two histograms: an upward-oriented histogram for concave-up change points, and a downward-oriented histogram for concave-down change points. We use these histograms as probabilistic locators of changes in slope (Figure 3).

The change point representations of the ATS2 and CO₂ time series are composed of a set of n specified change points $\{\mathbf{X}_i = (x_i, y_i) \mid i = 1, \dots, n\}$. We denote the vector of m time series observations o at time t $\{\mathbf{O}_l = (t_l, o_l) \mid l = 1, \dots, m\}$, and the scalar residual term J between observations and the linear interpolation between change points f_y :

$$J(\mathbf{X}_i) = \mathbf{R}^T \mathbf{C}^{-1} \mathbf{R}; \mathbf{r}_l = (f_y(t_l) - o_l)_l \quad (1)$$

45 where \mathbf{R} is the vector of residuals at each data point with components r_l and \mathbf{C} is the covariance matrix of the residuals. The ATS2 series contains 700 data points, and the WD CO₂ series contains 320, each of which is considered in the residuals.

We fix $x_0 = t_0$ and $x_n = t_l$; i.e. the x-values of the first and last change points are fixed to the first and last x-values of the observation vector, with the y-values allowed to vary. The remaining points are allowed to vary freely in both dimensions.

2.3.1 Estimating the covariance matrix \mathbf{C} : treating uncertainty and noise

Our method fits time series with piecewise linear functions, and the residual vector thus accounts for any variability that cannot be represented by these fits. Paleoclimate time series, like the CO₂ and ATS2 series used here, typically contain autocorrelated noise (see Mudelsee (2002), for example) which cannot be accurately represented by a piecewise linear function. Weighting the
 5 residuals of a cost-function based formulation by a properly estimated inverse covariance matrix ensures that this autocorrelated noise is not overfitted, and can improve the balance of precision and accuracy of the fits.

Our time series contain two potential sources of uncertainty: measurement or observational uncertainty, related with the creation of the data series, and modeling uncertainty, related to the residuals. We formulate a separate covariance matrix to account for each source of uncertainty. These matrices are then summed to form \mathbf{C} . We assume the first source of uncertainty
 10 to be uncorrelated in time (i.e. a white noise process). Thus, the associated covariance matrix \mathbf{C}_{meas} is diagonal, and the diagonal elements \mathbf{C}_{jj} are each equal to the variance of observation o_j , σ_j^2 , as estimated during the measurement process.

The covariance matrix of the modeling uncertainty, which we denote \mathbf{C}_{mod} , is more complicated, since the residual vector contains any autocorrelated noise in the time series that is not accounted for by the piecewise linear fits. Additionally, the time series contain outliers with respect to these linear fits, and these can impact any non-robust estimate of covariance. Finally,
 15 an initial idea of the model must be used to calculate residuals, and thus estimate their covariance. These challenges can be circumvented when data resolution is low enough to assume that residuals are uncorrelated, as in Parrenin et al. (2013), however, including the covariance matrix allows us to make use of noisy, high-resolution data.

We arrive at an initial model by running a MH simulation in which \mathbf{C} is assumed equal to the identity matrix, and select the best fit of this run. Note that \mathbf{C}_{meas} is not taken into account at this point, since we require an independent estimate of \mathbf{C}_{mod} .
 20 At this point, covariance could be estimated directly, but tests indicated that this method was not robust, making the covariance matrix estimate sensitive to outliers and to the initial model fit. Our CO₂ data are unevenly spaced in time, and developing a covariance matrix using the traditional covariance estimator would require some form of interpolation, which can introduce substantial error.

The residuals with respect to the initial model are instead used to fit an AR(1) model (Robinson, 1977; Mudelsee, 2002) which treats the autocorrelation between a pair of residuals r_i and r_{i-1} as a function of the separation between the two data points in time $t_i - t_{i-1}$. The Robinson (1977) / Mudelsee (2002) model is expressed:

$$r_i = r_{i-1} \cdot a^{t_i - t_{i-1}} \quad (2)$$

where the constant a determines the correlation between two residuals separated by $t_i - t_{i-1}$ units of time, and minimizing the loss function:

$$S(a) = \sum_{i=1}^n \{r_i - r_{i-1} \cdot a^{t_i - t_{i-1}}\} \quad (3)$$

allows us to estimate a . We do so using a nonlinear least-squares estimate with L1-norm regularization to provide a robust estimate (Chang and Politis, 2016). We confirm the validity of the AR(1) hypothesis by comparing r_i with $r_{i-1} \cdot a^{t_i - t_{i-1}}$ (Supplement). Given that the AR(1) hypothesis is accurate, we can use a to calculate the theoretical correlation between two residuals, and construct a correlation matrix \mathbf{K} and the model covariance matrix \mathbf{C}_{mod} as follows:

$$\mathbf{C}_{mod} = \sigma_{mod}^2 \mathbf{K}; \mathbf{K}_{ij} = a^{t_j - t_i} \quad (4)$$

where σ_{mod}^2 is the variance of the modeling error, assumed constant and estimated using a robust estimator as $(IQR(\mathbf{R})/1.349)^2$. Finally, the covariance matrix of the residuals \mathbf{C} is calculated as:

$$\mathbf{C} = \mathbf{C}_{mod} + \mathbf{C}_{meas}. \quad (5)$$

Rather than inverting the covariance matrix, we use Cholesky and LU decompositions to solve for the cost function value J , as in Parrenin et al. (2015).

2.4 Estimating the posterior probability density

In general, the probability density of the change points cannot be assumed to follow any particular distribution, as short-timescale variations of the time series may lead to multiple modes or heavy tails, for example. Thus, stochastic methods, which are best adapted to exploring general probability distributions (for example, Tarantola (2005)), are suited to our problem.

To tackle the large computation time required for traditional MH sampling, we apply the ensemble sampler developed by Goodman and Weare (2010) (GW) as implemented in the python emcee library (Foreman-Mackey et al., 2013). This sampler adapts the MH algorithm so that multiple model walkers can explore the probability distribution at once, making the algorithm parallelizable. It has the advantage of being affine invariant: that is, steps are adapted to the scale of the posterior distribution in a given direction.

We make histograms of the probable timings of 8 major change points for the WD CO₂ and AT2 series. The choice of 8 points is not entirely arbitrary: it reflects our goal of investigating millennial-scale variability (8 points allows for approximately one point per two millenia over the study period). This choice is subjective, but our method is not particularly sensitive to the number of change points. Since fits need not be perfect to be accepted in the stochastic simulation, we may estimate more or less peaks of high probability than the number of points used in the linear representation, and probability distributions of simulations with 8 and 10 points are rather similar (Supplementary Materials). The results of the 8-point simulation are shown in Figure 3. The most probable timings are identified by probability peaks, or modes. We avoid comparing incoherent modes by separating changes by the sign of the second derivative of the fits. Further details of the simulations are given in the supplement.

We implement a probability threshold to select significant change points. 94.9% of the histogram bins have (normalized) values below 0.0003—the value we select for the threshold. This threshold does not, on the other hand, evaluate significance in the sense of comparison with a null hypothesis. A simple null hypothesis could be that the series are equally well-represented by segments placed anywhere on the interval, in time, with y-axis values approximately corresponding to the data. We randomly generate 1000 points along the time intervals for both series, and calculate y-axis values for each point by linearly interpolating between data points at the respective x-value. We can thus create upward-facing and downward-facing histograms that reflect the approximate slopes of the series at any given time, but that effectively consider any change point timing to be appropriate. The bin values of the resulting normalized histograms do not surpass 0.0002. We choose the higher of these two estimates of significance, and consider peaks to be significant when the threshold is approximately met (within $\pm 2.5 \cdot 10^{-5}$) or clearly passed. The choice of this threshold over the lower threshold is ultimately arbitrary, and allowing for a buffer zone around the threshold reflects both this arbitrariness and the small uncertainty resulting from the stochastic nature of the histograms.

2.5 Phasing

We estimate ρ_{lead}^{ATS2} , the probability that AT2 leads CO₂ over a given interval, as

$$\rho_{lead}^{ATS2} = (\rho_x^{ATS2} \circ \rho_x^{CO_2}) \star \rho^{chron}, \quad (6)$$

where ρ_x^{ATS2} is the probability of a change point at time x for AT2, $\rho_x^{CO_2}$ is the probability of a change point at time x for CO₂, \circ is the cross-correlation operator, which is used to calculate the probability of the difference between two variables, and \star is the convolution operator, which is used to calculate the probability of the sum of two variables. ρ^{chron} is the probability distribution of the chronological uncertainty between the two records, which we take to be Gaussian centered on 0, with standard deviation $\sigma = \sigma_{chron}$ (shown in Figure 3). The intervals associated with each change point are given in Figure 6.

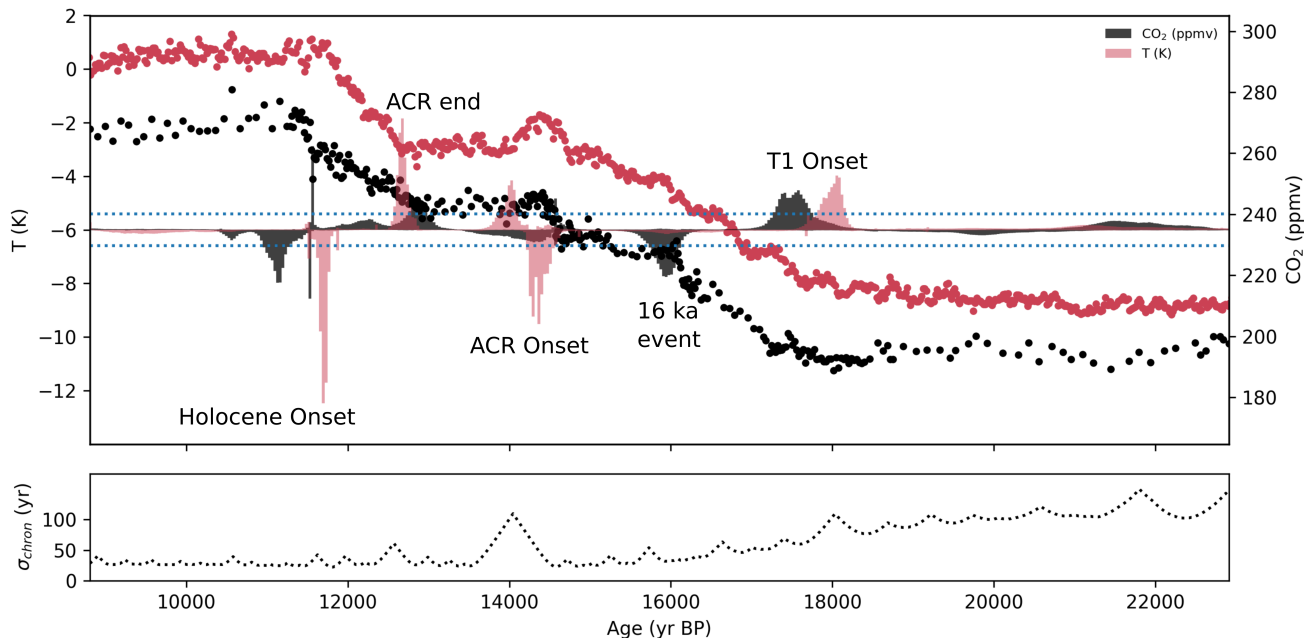


Figure 3. Upper panel: Atmospheric CO₂ (black) and ATS2 (red) placed on a common time scale, with the normalized histograms of probable change points (8 points). Histograms are plotted downward-oriented when the rate of change decreases and upward-oriented when it increases (same colors, y-axis not shown). Probabilities are normalized so that the integrated probability for a given histogram sums to 1, and range from 0 (center) to 0.004 (top/bottom). The 0.0003 probability threshold is marked by dotted blue lines. In four distinct time intervals, both series show concurrent probable change points. Lower panel: Chronological uncertainty, taken as the sum of the Δ age uncertainties and the uncertainty estimate for our volcanic synchronization.

3 Results and discussion

3.1 Change point timings

30 The change point histograms for the ATS2 and CO₂ time series in Figure 3 confirm that the millennial-scale changes in the two series were largely coherent. We identify four major changes in trend which surpass the 95% confidence interval for both series: the onset of the deglaciation from 18.2 to 17.2 ka B1950; the onset of the Antarctic Cold Reversal (ACR) at around 14.5 ka, the ACR end between 12.9 and 12.65, and the Holocene onset, at approximately 11.5 ka. For each of these four changes, we calculate the probability of a lead or lag. Two additional change points, one for CO₂ centered at approximately 16 ka, and
 35 a second change point for the temperature series after the ACR onset, centered at 14 ka, are also significant but do not have significant counterparts in the other series. Two abrupt, centennial-scale rises in CO₂, one at the ACR onset and before the Holocene onset, are visible in the histograms as narrow peaks. These changes have been identified in the WD CO₂ record by Marcott et al. (2014), though the beginning of a third such rapid change before 16ka is not detected here.

The deglaciation onset begins with a large, positive change point mode for Antarctic temperature, centered around 18.1 ka.

40 The corresponding change point for the CO₂ series is centered around 17.6 ka.

The CO₂ rise peaks at around 16 ka, identified by a downward-oriented probability peak, which has no significant counterpart in the temperature series. This peak is followed by a brief plateau in CO₂ concentrations, before a gradual, accelerating resumption of the increase.

An abrupt CO₂ rise preceded the Antarctic Cold Reversal. Two narrow spikes in probability, upward- and downward- facing,

45 near 14.58 ka, appear to represent this rise, the downward peak just reaching the significance threshold. The broad tail of the downward-facing CO₂ change point peaks again at around 14.35 ka. On its own, the second mode does not reach the significance threshold, but it appears to reflect further methodological uncertainty with respect to the timing of the millennial-scale change in CO₂. An unambiguous negative temperature change also occurs at around 14.35 ka, roughly concurrent with the downward CO₂ change point. Antarctic temperature began to descend rapidly after the ACR onset, finally stabilizing at the concave-up change point identified by the mode centered on 14.02 ka. No corresponding change point is detected for CO₂.

The ACR termination is represented by significant modes in both series. An increase in CO₂ began at the peak occurring around 12.88 ka, while the AT2S increase is centered at 12.65 ka, approximately.

The Holocene onset is well-defined in the AT2S series, with a large mode centered at 11.7 ka. The probability peaks in the

5 CO₂ series are remarkably similar to those identified at the ACR onset. A rapid rise in CO₂ is represented by narrow peaks from 11.57 to 11.53 ka. A second, broad mode, representing further methodological uncertainty about the timing of the change of the long-term, millennial scale trend. Our method cannot specify which mode better represents the change, and both must be considered.

As a second test of the timings of millennial-scale events, we use our method to fit filtered versions of the AT2S and WAIS

10 Divide CO₂ data. A Savitsky-Golay filter, designed to have an approximate cutoff periodicity of 500 years, is applied to the two records. In the two filtered series, the sub-millennial scale AR(1) noise present in the original series should be essentially removed. As such, fitting change points to these two series, assuming the residuals to be uncorrelated, provides a second form of verification of the appropriateness of the covariance matrix we use to fit the raw data.

Figure 4 shows the Savitsky-Golay filtered CO₂ and AT2S time series, and the corresponding change point histograms. The

15 four major changes identified in both series, at the T1 onset, the ACR onset, the ACR end, and Holocene onset, are similar in shape and center to the fits of the raw data. However, there are two notable differences between the two fits. First, the spikes representing centennial-scale CO₂ rises before the ACR and Holocene onsets are entirely removed. This is not surprising, given that the Savitsky-Golay filters are designed to remove all variability with periodicities less than 500 years, whereas the covariance matrix applied to the fits of the raw data only treats AR(1) correlated noise. Finally, the probability of the

20 post-ACR change in AT2S is considerably smaller for the filtered series. Savitsky-Golay filtering has its own drawbacks—data reinterpolation is required, for example, and propagating measurement uncertainty becomes difficult. However, the similarity of the two results supports our fits of the raw data.

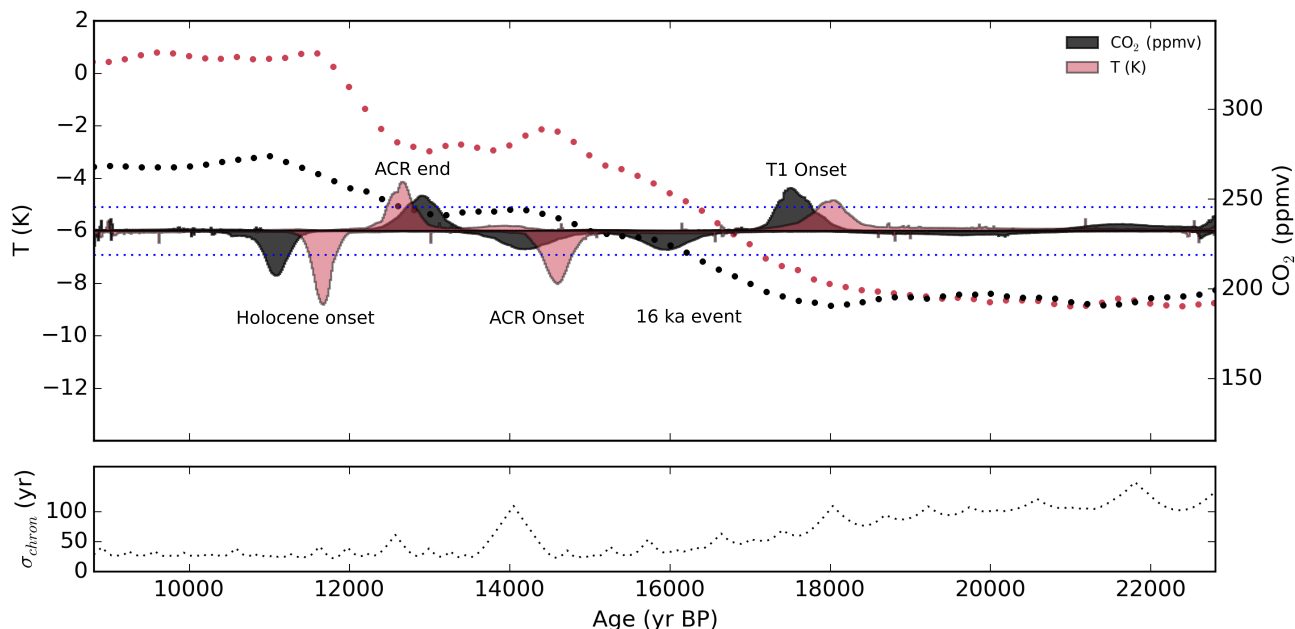


Figure 4. Upper panel: Savitsky-Golay filtered atmospheric CO₂ (black) and ATs2 (red) placed on a common time scale, with the normalized histograms of probable change points (8 points). Histograms are plotted downward-oriented when the rate of change decreases and upward-oriented when it increases (same colors, y-axis not shown, probabilities range from 0 (center) to 0.0024 (top/bottom)). The 0.0003 probability threshold is marked by dotted blue lines for reference, but is not applied here. Lower panel: Chronological uncertainty, taken as the sum of the Δ age uncertainties and the uncertainty estimate for our volcanic synchronization.

3.2 Change point timings for individual temperature records

Fits of each of the regional temperature records, corrected for source isotopic variations (Bintanja et al., 2013) are shown in figure 5. These fits should still be interpreted cautiously, as additional information included in the isotopic records used to calculate temperature—the signal of ice sheet elevation change, for example—are not corrected for. The comparison of these fits provides an initial, exploratory picture of potential regional differences in climate change during the last termination.

Of the four changes identified as coherent between the temperature stack and CO₂, those at the deglaciation onset, the ACR end, and the Holocene onset are expressed as significant probability peaks in all five records. Some ambiguity appears to exist about the timing of the ACR onset in the EDML record. It is expressed by a rather broad, non-significant probability mode extending between 16ka and 14ka, though a significant spike at 14ka marks the downturn seen in the other records. The ACR onset is significant and well-defined in all of the five other records.

The WAIS Divide record is, notably, the only isotopic record in our stack from the West Antarctic ice sheet. We could thus reasonably expect it to show considerably different trends from the other records. Indeed, a significant change in the WD temperature record occurs at 22 ka. This early change in the isotopic record was identified and confirmed to indeed be a

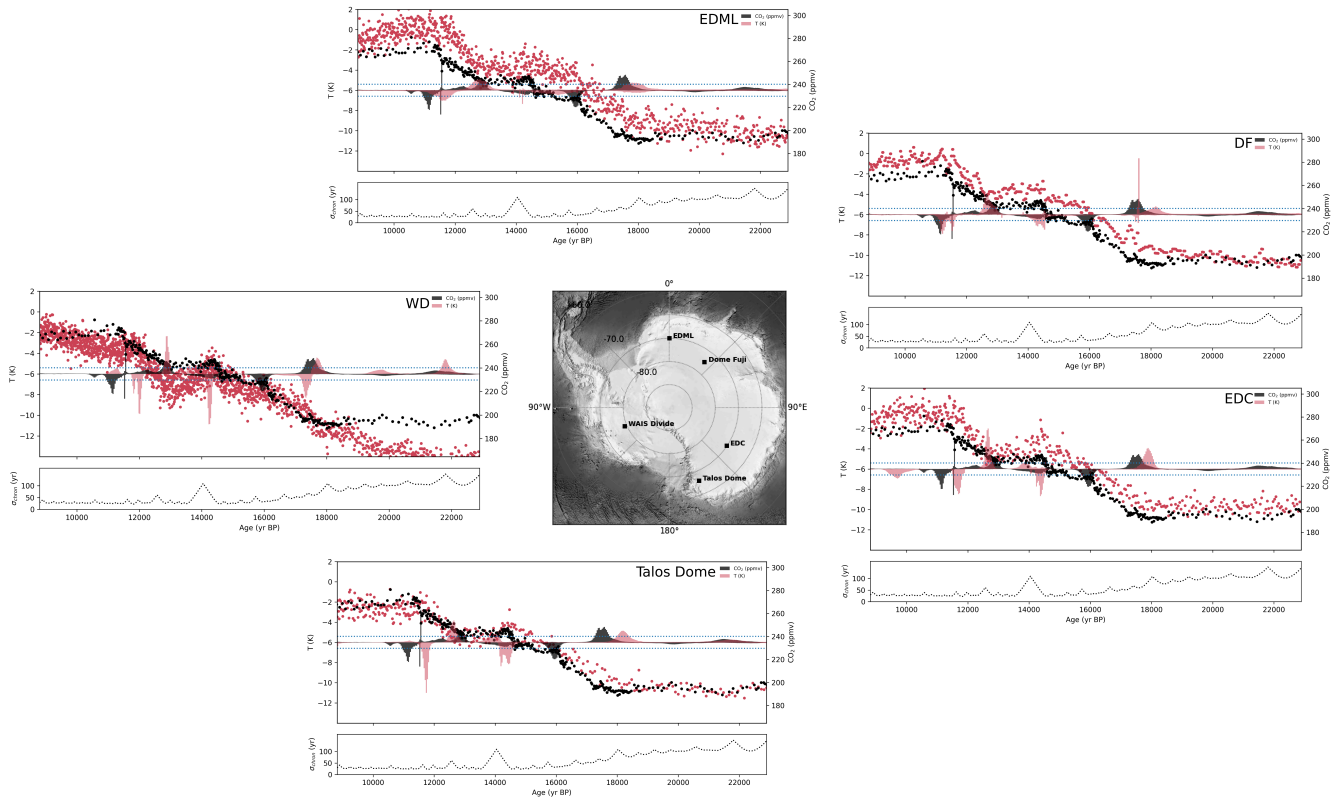


Figure 5. Atmospheric CO₂ (black) and source-corrected temperature records (red) placed on a common time scale, with the normalized histograms of probable change points (8 points) for each ice core used in the ATS2 stack; the locations of the drill sites are shown in the center. Details of the histogram plots are as in Figure 3.

temperature signal by Cuffey et al. (2016) using a borehole temperature record, though their study places the change at 21 ka. We confirm that the onset of the deglacial temperature rise in West Antarctica likely began as much as 4 ka before the onset of temperature rise in East Antarctica. Interestingly, the WD record also shows a temperature change point around 17.8 ka, expressed slightly later than in the other records and more synchronous with CO₂. This apparent acceleration of the temperature rise is followed by a significant downward-facing change point not seen in any of the other records. A difference appears to exist in timing at the Holocene onset as well, with temperature change at WD appearing to slightly precede temperature in the East Antarctic records, and the DF temperature change in particular appearing to occur more synchronously with CO₂.

3.3 Leads and lags

The probability densities of leads and lags at the coherent change points between ATS2 and CO₂ are shown in Figure 6. We then report the 1 σ standard deviation of the lead/lag, but this estimate must be applied with care where the lead probability is still multimodal, as is the case at the Holocene and ACR onsets.

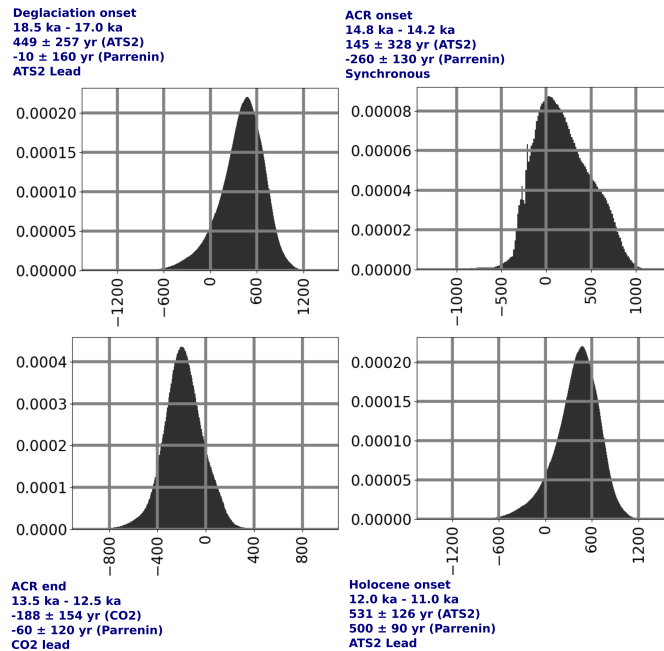


Figure 6. Probability density ρ (y-axis, normalized) of an ATS lead (x-axes, in years) at each of the selected change point intervals (noted on subfigures). Negative x-axis values indicate a CO₂ lead. In the text in each box, the name of the period, the time period in which the lead is calculated, the mean and standard deviation of the lead/lag density (μ and 1σ), and the leading variable are given.

ATS2 led CO₂ by 449 ± 257 years at the T1 onset. Given the large range of uncertainty, we cannot exclude the possibility of synchrony. At the ACR onset, the range of uncertainty (145 ± 328 years) that includes both the large relative chronological uncertainty and the ambiguity concerning the timing of the CO₂ change point, related to the large centennial scale variability near this point, does not allow us to identify a lead or lag. At the ACR end, CO₂ led ATS2, by 188 ± 154 years, but again, the possibility of synchrony cannot be excluded within 2σ .

At the Holocene onset, a CO₂ lag is certain. Calculating the phasing between 12.0 ka and 11.0 ka, we obtain an ATS2 lead of 531 ± 126 years.

If the end of the centennial-scale change in CO₂ coincides with the true millennial scale change, which appears visually plausible, the ATS2 lead is much smaller. However, considerable uncertainty with respect to the millennial-scale change is expressed by the second mode, and the estimate of 574 ± 143 is statistically more appropriate.

3.4 Discussion

- 10 Our results refine and complicate the timings and leads and lags identified by the most recent comparable studies (Parrenin et al., 2013; Pedro et al., 2012). We identify a CO₂ change point not treated in these studies at 16 ka, associated with the end of the centennial-scale rapid rise identified by Marcott et al. (2014), and an Antarctic temperature change point at 14 ka, neither of which have a counterpart in the other series.

During the major, multi-millennial scale changes which occur at T1 and Holocene onsets, Antarctic temperature likely led
15 CO₂ by several centuries. However, during the complex, centennial-scale change at the ACR onset, ATS was most likely
synchronous with CO₂, and at the end of the ACR, CO₂ leads temperature. Further, we do not identify an analog in CO₂ of the
marked temperature decrease in Antarctica after the ACR onset, or a temperature analog for the CO₂ change at 16ka, indicating
at least some degree of decoupling during these changes. Additionally, the CO₂ changes at the ACR and Holocene onsets are
overlaid with centennial-scale substructures. Finally, synchrony is within the 2 σ uncertainty range for each of the phasings,
20 with the exception of the Holocene onset.

The changes in CO₂ occurring at the ACR onset, ACR end and 11.6 ka and the Holocene onset have been identified to
correspond with changes in CH₄ (Marcott et al., 2014), which are thought to originate in tropical wetland sources (Chappellaz
et al., 1997; Fischer et al., 2008; Petrenko et al., 2009) and are indicative of Northern Hemisphere and low-latitude temperature
changes during the deglaciation (Shakun et al., 2012). Indeed, the CO₂ modes appear to demarcate the rapid changes in the
25 WD CH₄ record, shown in Figure 7.

The beginning of a gradual rise in CH₄ at around 18 ka appears to be near-synchronous with the T1 onset rise in Antarctic
temperature. This rise is not seen in Greenland paleotemperature records, where it may have been masked by AMOC-driven
wintertime cooling (Buizert et al., 2017) but it appears as well in proxy temperature stacks spanning both the Northern and
Southern 0° to 30° latitude bands (Shakun et al., 2012).

30 Tephra from Mt. Takahe, a stratovolcano located in West Antarctica, have been detected in Antarctic ice cores during a 192
year interval around 17.7 ka. It has been postulated that this eruption may have provoked changes to large-scale SH circulation
via ozone depletion, possibly triggering the transition between the gradual SH temperature rise beginning well before 18 ka
and the more rapid rise marking the deglaciation (McConnell et al., 2017). The CO₂ mode we find at the deglaciation is coeval
with this event within the range of dating uncertainty (Figure 7), and CH₄ visually appears to accelerate concurrently. However,
35 the cumulative probability of the ATS2 change point is much greater before 17.7 ka than after.

Though the T1 onset and the ACR end are both thought to originate in AMOC reductions (Marcott et al., 2014), our results
allow for the directionality of CO₂-ATS2 phasing to be reversed during the two events. CH₄ changes nearly synchronously
with CO₂ at both points, but the phasings are opposite in direction and different in magnitude. This hints at a complex coupling,
depending on conditions defined by multiple other variables and mechanisms, between CO₂ and Antarctic Temperature. Bauska
40 et al. (2016), for example, hypothesize that an earlier rise of CO₂ at 12.9 ka, driven by land carbon loss or SH westerly winds,
might have been superimposed on the millennial-scale trend.

The apparent decoupling between CO₂ and ATS2 at 16 ka also merits further discussion. None of the five isotopic records
show significant probability in this region, but the EDML record contains extremely broad uncertainty associated with the
significant ACR onset peak, stretching to 16 ka, which indicates that this portion of the EDML time series is indeed notably
45 different in shape from the other records, even if a clear signal is not identified at 16 ka by our method. EDML is located
geographically closer to the Atlantic than the other drilling sites, potentially positioning it to better record changes in AMOC
or the Atlantic water cycle during the climatic reorganization that occurred around 16 ka as detailed by Landais et al. (2018),
who also note the difference of the EDML record during this period. CO₂ and ATS2 are similarly apparently decoupled at

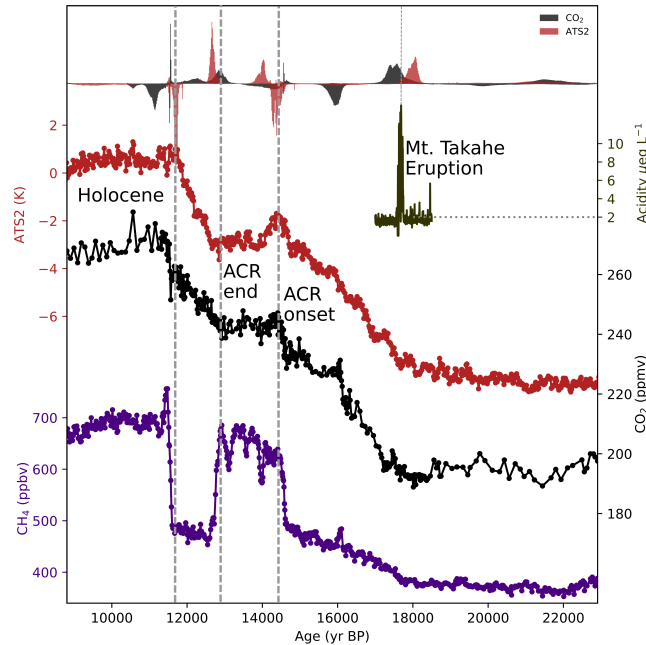


Figure 7. WD CO₂ and ATS2 change point histograms plotted with WD Acidity, ATS2, WD CO₂ and WD CH₄ series (top to bottom). Vertical lines are plotted to highlight select change point modes for the CO₂ (black) and ATS2 (red) series. CH₄ tracks changes in Northern Hemisphere climate. CO₂ modes correspond with rapid changes in CH₄ at the ACR end, ACR onset, 16 ka rise, and the rapid rise preceding the Holocene onset.

the temperature change point centered at 14 ka, and this point could be indicative of variability specific to the Pacific/Eastern Indian Ocean sectors, as it is present only in the TALOS Dome and EDC records, and slightly later, around 13.7 ka, in the WAIS Divide record, indicating a cooling trend after the ACR onset which is not clear in the DF or EDML series.

Within the range of uncertainty, our lead-lag estimates are only roughly consistent with those of Pedro et al. (2012) and Parrenin et al. (2013). The addition of the WD paleotemperature record and removal of the Vostok record from ATS2, the updated atmospheric CO₂ dataset, and our more generalized methodology are all, in part, responsible for the differences in computed time delays (SI). This testifies to the importance of data resolution, methodological development, and chronological accuracy in the determination of leads and lags.

4 Conclusions

Our study is a follow-up of the studies by Pedro et al. (2012) and Parrenin et al. (2013) on the leads and lags between atmospheric CO₂ and Antarctic temperature during the last deglacial warming. We refine the results of these studies by using the high resolution CO₂ record from WD; using the ice-air shift computed on WD; deriving a new Antarctic Temperature Stack composed of 5 volcanically synchronized ice core isotope records; and using a more precise and complete probabilis-

tic estimate to determine change points. Our methodology detects four major common break points in both time series. The phasing between CO₂ and Antarctic climate is close but variable, with phasing ranging from a centennial-scale CO₂ lead, to
15 synchrony, to a centennial-scale lead of Antarctic climate. This variability suggests complex mechanisms of coupling that can be modulated by external forcing.

We additionally explore the hypothesis of regional difference in temperature change in West Antarctica. Though the use of individual isotopic temperature records is complicated by the regional external influences on the isotopes, we confirm that the deglacial temperature rise did not occur homogeneously across the Antarctic continent, with significant differences existing
20 between the WAIS Divide and East Antarctic records at the onset of the termination, and smaller potential differences occurring between the East Antarctic records.

Hypotheses of relationships between these events should now be reinvestigated with modeling studies. The relationship between CO₂ and Antarctic temperature on longer timescales and during other periods of rapid climate change is also of interest, as is the investigation of the role CO₂ in global temperature change. Additional high-resolution West Antarctic pale-
25 otemperature records would allow for a robust investigation of regional differences between West and East Antarctica, and our analysis at the Holocene onset could be improved with continued high-resolution CO₂ measurements through the beginning of the Holocene. Finally, the continued measurement of high-resolution ice core CO₂ records is essential to understand the relationship between CO₂ and global and regional temperature during the last 800,000 years.

Code and data availability.

30 *Acknowledgements.* We thank Michael Sigl, Jinhwa Shin, Emmanuel Witrant and Amaelle Landais for their support and great help discussing this work and Mirko Severi for his EDC data and support with the volcanic synchronisation. This work is supported by the Fondation Ars et Cuttoli, and by the LEFE IceChrono and CO₂Role projects.

Competing interests. The authors declare that no competing interests are present for this study.

References

- 35 Barnola, J.-M., Pimienta, P., Raynaud, D., and Korotkevich, Y. S.: CO₂-climate relationship as deduced from the Vostok ice core: a re-examination based on new measurements and on a re-evaluation of the air dating, *Tellus B*, 43, 83–90, 1991.
- Bauska, T. K., Baggenstos, D., Brook, E. J., Mix, A. C., Marcott, S. A., Petrenko, V. V., Schaefer, H., Severinghaus, J. P., and Lee, J. E.: Carbon isotopes characterize rapid changes in atmospheric carbon dioxide during the last deglaciation, *Proceedings of the National Academy of Sciences*, 113, 3465–3470, 2016.
- 40 Berger, A.: Long-term variations of daily insolation and Quaternary climatic changes, *Journal of the atmospheric sciences*, 35, 2362–2367, 1978.
- Bintanja, R., Van Oldenborgh, G., Drijfhout, S., Wouters, B., and Katsman, C.: Important role for ocean warming and increased ice-shelf melt in Antarctic sea-ice expansion, *Nature Geoscience*, 6, 376, 2013.
- Buizert, C. and Severinghaus, J. P.: Dispersion in deep polar firn driven by synoptic-scale surface pressure variability, *The Cryosphere*, 10, 2099–2111, 2016.
- 45 Buizert, C., Cuffey, K., Severinghaus, J., Baggenstos, D., Fudge, T., Steig, E., Markle, B., Winstrup, M., Rhodes, R., Brook, E., et al.: The WAIS Divide deep ice core WD2014 chronology—Part 1: Methane synchronization (68–31 ka BP) and the gas age–ice age difference, *Climate of the Past*, 11, 153–173, 2015.
- Buizert, C., Keisling, B. A., Box, J. E., He, F., Carlson, A. E., Sinclair, G., and DeConto, R. M.: Greenland-Wide Seasonal Temperatures During the Last Deglaciation, *Geophysical Research Letters*, pp. n/a–n/a, doi:10.1002/2017GL075601, <http://dx.doi.org/10.1002/2017GL075601>, 2017GL075601, 2017.
- Caillon, N., Severinghaus, J. P., Jouzel, J., Barnola, J.-M., Kang, J., and Lipenkov, V. Y.: Timing of atmospheric CO₂ and Antarctic temperature changes across Termination III, *Science*, 299, 1728–1731, 2003.
- 5 Chang, C. C. and Politis, D. N.: Robust autocorrelation estimation, *Journal of Computational and Graphical Statistics*, 25, 144–166, 2016.
- Chappellaz, J., Blunier, T., Kints, S., Dällenbach, A., Barnola, J.-M., Schwander, J., Raynaud, D., and Stauffer, B.: Changes in the atmospheric CH₄ gradient between Greenland and Antarctica during the Holocene, *J Geophys Res Atmos*, 102, 15 987–15 997, 1997.
- Cuffey, K. M., Clow, G. D., Steig, E. J., Buizert, C., Fudge, T., Koutnik, M., Waddington, E. D., Alley, R. B., and Severinghaus, J. P.: 10 Deglacial temperature history of West Antarctica, *Proc Natl Acad Sci U S A*, 113, 14 249–14 254, 2016.
- Fischer, H., Behrens, M., Bock, M., Richter, U., Schmitt, J., Loulergue, L., Chappellaz, J., Spahni, R., Blunier, T., Leuenberger, M., et al.: Changing boreal methane sources and constant biomass burning during the last termination, *Nature*, 452, 864, 2008.
- Foreman-Mackey, D., Hogg, D. W., Lang, D., and Goodman, J.: Emcee: The MCMC Hammer, *Publications of the Astronomical Society of the Pacific*, 125, 306, doi:10.1086/670067, 2013.
- 15 Fujita, S., Parrenin, F., Severi, M., Motoyama, H., and Wolff, E.: Volcanic synchronization of Dome Fuji and Dome C Antarctic deep ice cores over the past 216 kyr, *Climate of the Past*, 11, 1395, 2015.
- Goodman, J. and Weare, J.: Ensemble samplers with affine invariance, *Comm app math comp sci*, 5, 65–80, 2010.
- Hays, J. D., Imbrie, J., and Shackleton, N. J.: Variations in the Earth’s orbit: pacemaker of the ice ages, *Science*, 194, 1121–1132, 1976.
- Johnsen, S., Dansgaard, W., and White, J.: The origin of Arctic precipitation under present and glacial conditions, *Tellus B*, 41, 452–468, 20 1989.
- Jones, J. M., Gille, S. T., Goosse, H., Abram, N. J., Canziani, P. O., Charman, D. J., Clem, K. R., Crosta, X., De Lavergne, C., Eisenman, I., et al.: Assessing recent trends in high-latitude Southern Hemisphere surface climate, *Nature Climate Change*, 6, 917, 2016.

- Jouzel, J., Masson-Delmotte, V., Cattani, O., Dreyfus, G., Falourd, S., Hoffmann, G., Minster, B., Nouet, J., Barnola, J.-M., Chappellaz, J., et al.: Orbital and millennial Antarctic climate variability over the past 800,000 years, *Science*, 317, 793–796, 2007.
- 25 Kawamura, K., Parrenin, F., Lisiecki, L., Uemura, R., Vimeux, F., Severinghaus, J. P., Hutterli, M. A., Nakazawa, T., Aoki, S., Jouzel, J., et al.: Northern Hemisphere forcing of climatic cycles in Antarctica over the past 360,000 years, *Nature*, 448, 912–916, 2007.
- Lambert, F., Bigler, M., Steffensen, J. P., Hutterli, M., and Fischer, H.: Centennial mineral dust variability in high-resolution ice core data from Dome C, Antarctica, *Climate of the Past*, 8, 609–623, 2012.
- Landais, A., Capron, E., Masson-Delmotte, V., Toucanne, S., Rhodes, R., Popp, T., Vinther, B., Minster, B., and Prié, F.: Ice core evidence
30 for decoupling between midlatitude atmospheric water cycle and Greenland temperature during the last deglaciation, *Climate of the Past*, 14, 1405–1415, 2018.
- Lisiecki, L. and Raymo, M.: A Plio-Pleistocene stack of 57 globally distributed benthic 0126-026180 records, *Paleoceanography*, 20, 2005.
- Lorius, C. and Merlivat, L.: Distribution of mean surface stable isotopes values in East Antarctica; observed changes with depth in coastal area, Tech. rep., CEA Centre d'Etudes Nucleaires de Saclay, 1975.
- 35 Loulergue, L., Parrenin, F., Blunier, T., Barnola, J.-M., Spahni, R., Schilt, A., Raisbeck, G., and Chappellaz, J.: New constraints on the gas age-ice age difference along the EPICA ice cores, 0-50 kyr, *Climate of the Past*, 3, 527–540, 2007.
- Lüthi, D., Le Floch, M., Bereiter, B., Blunier, T., Barnola, J.-M., Siegenthaler, U., Raynaud, D., Jouzel, J., Fischer, H., Kawamura, K., et al.: High-resolution carbon dioxide concentration record 650,000–800,000 years before present, *Nature*, 453, 379–382, 2008.
- Marcott, S. A., Bauska, T. K., Buizert, C., Steig, E. J., Rosen, J. L., Cuffey, K. M., Fudge, T., Severinghaus, J. P., Ahn, J., Kalk, M. L., et al.:
40 Centennial-scale changes in the global carbon cycle during the last deglaciation, *Nature*, 514, 616–619, 2014.
- Masson-Delmotte, V., Schulz, M., Abe-Ouchi, A., Beer, J., Ganopolski, A., González Rouco, J., Jansen, E., Lambeck, K., Luterbacher, J., Naish, T., Osborn, T., Otto-Bliesner, B., Quinn, T., Ramesh, R., Rojas, M., Shao, X., and Timmermann, A.: Information from Paleoclimate Archives, in: *Climate Change 2013: The Physical Science Basis. Contribution of Working Group I to the Fifth Assessment Report of the Intergovernmental Panel on Climate Change*, edited by Stocker, T., Qin, D., Plattner, G.-K., Tignor, M., Allen, S., Boschung, J., Nauels, A., Xia, Y., Bex, V., and Midgley, P., book section 5, p. 383–464, Cambridge University Press, Cambridge, United Kingdom and New York, NY, USA, doi:10.1017/CBO9781107415324.013, www.climatechange2013.org, 2013.
- McConnell, J. R., Burke, A., Dunbar, N. W., Köhler, P., Thomas, J. L., Arienzo, M. M., Chellman, N. J., Maselli, O. J., Sigl, M., Adkins, J. F., et al.: Synchronous volcanic eruptions and abrupt climate change 17.7 ka plausibly linked by stratospheric ozone depletion, *Proc Natl Acad Sci U S A*, p. 201705595, 2017.
- Monnin, E., Indermühle, A., Dällenbach, A., Flückiger, J., Stauffer, B., Stocker, T. F., Raynaud, D., and Barnola, J.-M.: Atmospheric CO₂ concentrations over the last glacial termination, *Science*, 291, 112–114, 2001.
- Mudelsee, M.: TAUEST: A computer program for estimating persistence in unevenly spaced weather/climate time series, *Computers & Geosciences*, 28, 69–72, 2002.
- 5 NorthGRIP Project Members: High-resolution record of Northern Hemisphere climate extending into the last interglacial period, *Nature*, 431, 147–151, 2004.
- Parrenin, F., Barker, S., Blunier, T., Chappellaz, J., Jouzel, J., Landais, A., Masson-Delmotte, V., Schwander, J., and Veres, D.: On the gas-ice depth difference (Δ depth) along the EPICA Dome C ice core, *Climate of the Past*, 8, 1239–1255, 2012.
- Parrenin, F., Masson-Delmotte, V., Köhler, P., Raynaud, D., Paillard, D., Schwander, J., Barbante, C., Landais, A., Wegner, A., and Jouzel, J.:
10 Synchronous change of atmospheric CO₂ and Antarctic temperature during the last deglacial warming, *Science*, 339, 1060–1063, 2013.

- Parrenin, F., Bazin, L., Capron, E., Landais, A., Lemieux-Dudon, B., and Masson-Delmotte, V.: IceChrono1: a probabilistic model to compute a common and optimal chronology for several ice cores, *Geoscientific Model Development*, 8, 1473–1492, 2015.
- Pedro, J. B., Rasmussen, S. O., and van Ommen, T. D.: Tightened constraints on the time-lag between Antarctic temperature and CO₂ during the last deglaciation, *Climate of the Past*, 8, 1213–1221, 2012.
- 15 Pedro, J. B., Bostock, H. C., Bitz, C. M., He, F., Vandergoes, M. J., Steig, E. J., Chase, B. M., Krause, C. E., Rasmussen, S. O., Markle, B. R., et al.: The spatial extent and dynamics of the Antarctic Cold Reversal, *Nature Geoscience*, 9, 51, 2016.
- Petit, J.-R. and Delmonte, B.: A model for large glacial–interglacial climate-induced changes in dust and sea salt concentrations in deep ice cores (central Antarctica): Palaeoclimatic implications and prospects for refining ice core chronologies, *Tellus B*, 61, 768–790, 2009.
- Petrenko, V. V., Smith, A. M., Brook, E. J., Lowe, D., Riedel, K., Brailsford, G., Hua, Q., Schaefer, H., Reeh, N., Weiss, R. F., et al.: 14CH₄ measurements in Greenland ice: investigating last glacial termination CH₄ sources, *Science*, 324, 506–508, 2009.
- 20 Raynaud, D. and Siegenthaler, U.: Role of trace gases: the problem of lead and lag, *Global changes in the perspective of the past*, pp. 173–188, 1993.
- Raynaud, D., Jouzel, J., Barnola, J., Chappellaz, J., Delmas, R., and Lorius, C.: The ice record of greenhouse gases, *Science*, 259, 926–926, 1993.
- 25 Robinson, P.: Estimation of a time series model from unequally spaced data, *Stochastic Processes and their Applications*, 6, 9–24, 1977.
- Shakun, J. D., Clark, P. U., He, F., Marcott, S. A., Mix, A. C., Liu, Z., Otto-Bliesner, B., Schmittner, A., and Bard, E.: Global warming preceded by increasing carbon dioxide concentrations during the last deglaciation, *Nature*, 484, 49–54, 2012.
- Sigl, M., Fudge, T., Winstrup, M., Cole-Dai, J., Ferris, D., McConnell, J., Taylor, K., Welten, K., Woodruff, T., Adolphi, F., et al.: The WAIS Divide deep ice core WD2014 chronology-Part 2: Annual-layer counting (0–31 ka BP), *Climate of the Past*, 11, 3425–3474, 2016.
- 30 Sowers, T., Bender, M., Raynaud, D., and Korotkevich, Y. S.: $\delta^{15}\text{N}$ of N₂ in air trapped in polar ice: A tracer of gas transport in the firm and a possible constraint on ice age-gas age differences, *J Geophys Res Atmos*, 97, 15 683–15 697, 1992.
- Tarantola, A.: *Inverse problem theory*, SIAM, 2005.
- WAIS Divide Project Members and others: Onset of deglacial warming in West Antarctica driven by local orbital forcing, *Nature*, 500, 440–444, 2013.
- 35 Williams, D., Peck, J., Karabanov, E., Prokopenko, A., Kravchinsky, V., King, J., and Kuzmin, M.: Lake Baikal record of continental climate response to orbital insolation during the past 5 million years, *Science*, 278, 1114–1117, 1997.
- Zhang, H., Griffiths, M. L., Huang, J., Cai, Y., Wang, C., Zhang, F., Cheng, H., Ning, Y., Hu, C., and Xie, S.: Antarctic link with East Asian summer monsoon variability during the Heinrich Stadial–Bølling interstadial transition, *Earth Planet. Sci. Lett.*, 453, 243–251, 2016.